Science Advances
AAAS

advances.sciencemag.org/cgi/content/full/6/14/eaaz4729/DC1

Supplementary Materials for

Australopithecus afarensis endocasts suggest ape-like brain organization and prolonged brain growth

Philipp Gunz*, Simon Neubauer, Dean Falk, Paul Tafforeau, Adeline Le Cabec, Tanya M. Smith, William H. Kimbel, Fred Spoor, Zeresenay Alemseged

*Corresponding author. Email: gunz@eva.mpg.de

Published 1 April 2020, *Sci. Adv.* **6**, eaaz4729 (2020)
DOI: 10.1126/sciadv.aaz4729

The PDF file includes:

Figs. S1 to S8
Tables S1 to S2
Legend for data file S1
References

Other Supplementary Material for this manuscript includes the following:

(available at advances.sciencemag.org/cgi/content/full/6/14/eaaz4729/DC1)

Data file S1

Supplementary Materials

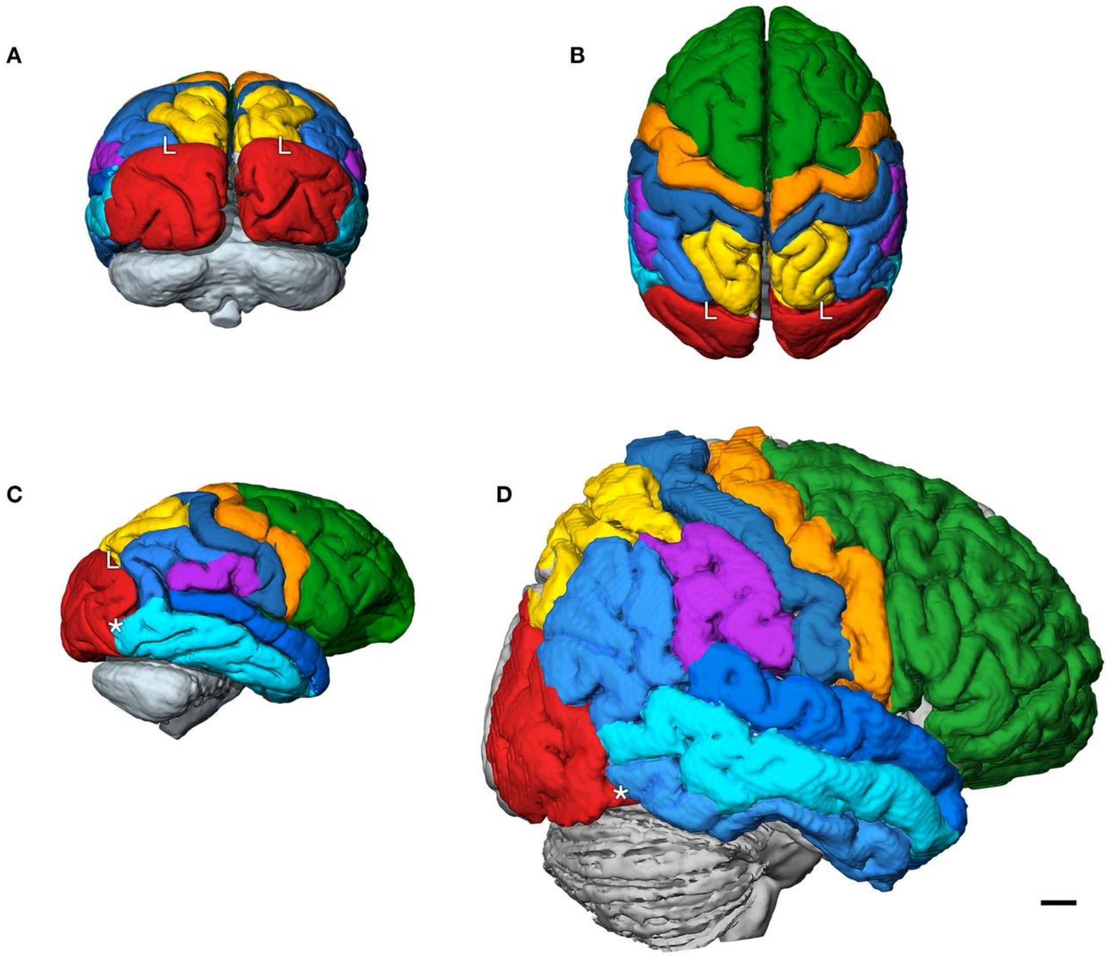

Fig. S1. Different brain organization in apes and humans. Whereas the lunate sulcus (L) is a prominent structure on ape brains, the morphology of the occipital lobe (red) is highly variable in *Homo sapiens*, who rarely display a "true" lunate sulcus. (**A-C**) Segmentation of a chimpanzee brain based on an MRI scan, in posterior, superior, and lateral views. (**D**) Modern human brain in lateral view. Some researchers have used the "occipital notch" in *H. sapiens* brains as the structure corresponding to the inferior and lateral end of the ape lunate sulcus (*58*, *59*). The asterisk in (**C**) points to the inferior and lateral end of the lunate sulcus in *P. troglodytes*; the asterisk in (D) to the corresponding structure in *H. sapiens*. Scale bar is 1 cm.

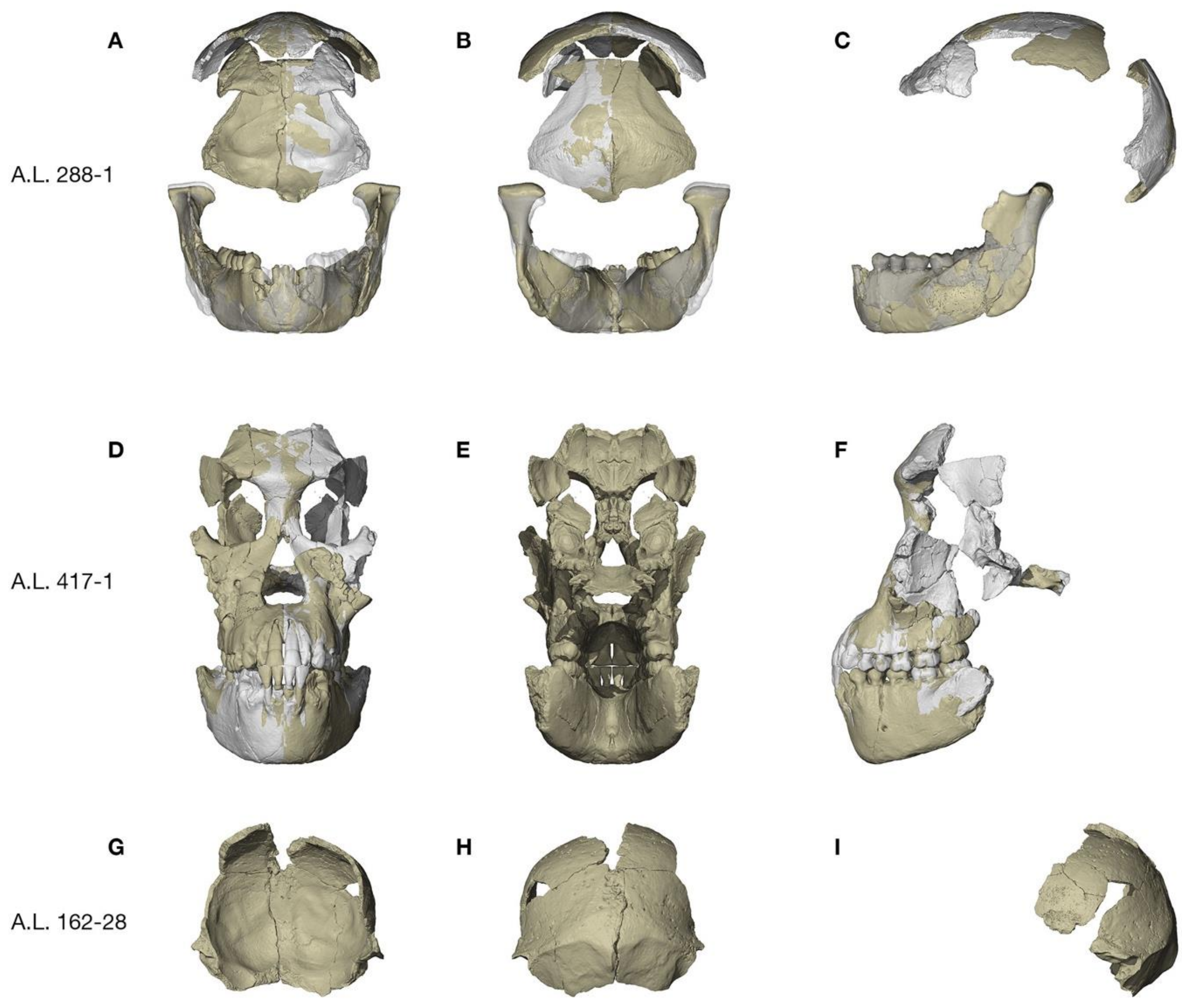

Fig. S2. Size comparison of small *A. afarensis* adults. (**A**-**C**) Reconstruction of A.L. 288-1 in anterior, posterior, and lateral view. Mirrored surfaces are shown in gray. (**D-F**) Reconstruction of A.L. 417-1 in anterior, posterior, and lateral view. (**G**-**I**) Original surface of A.L. 162-28 in anterior, posterior, and lateral view.

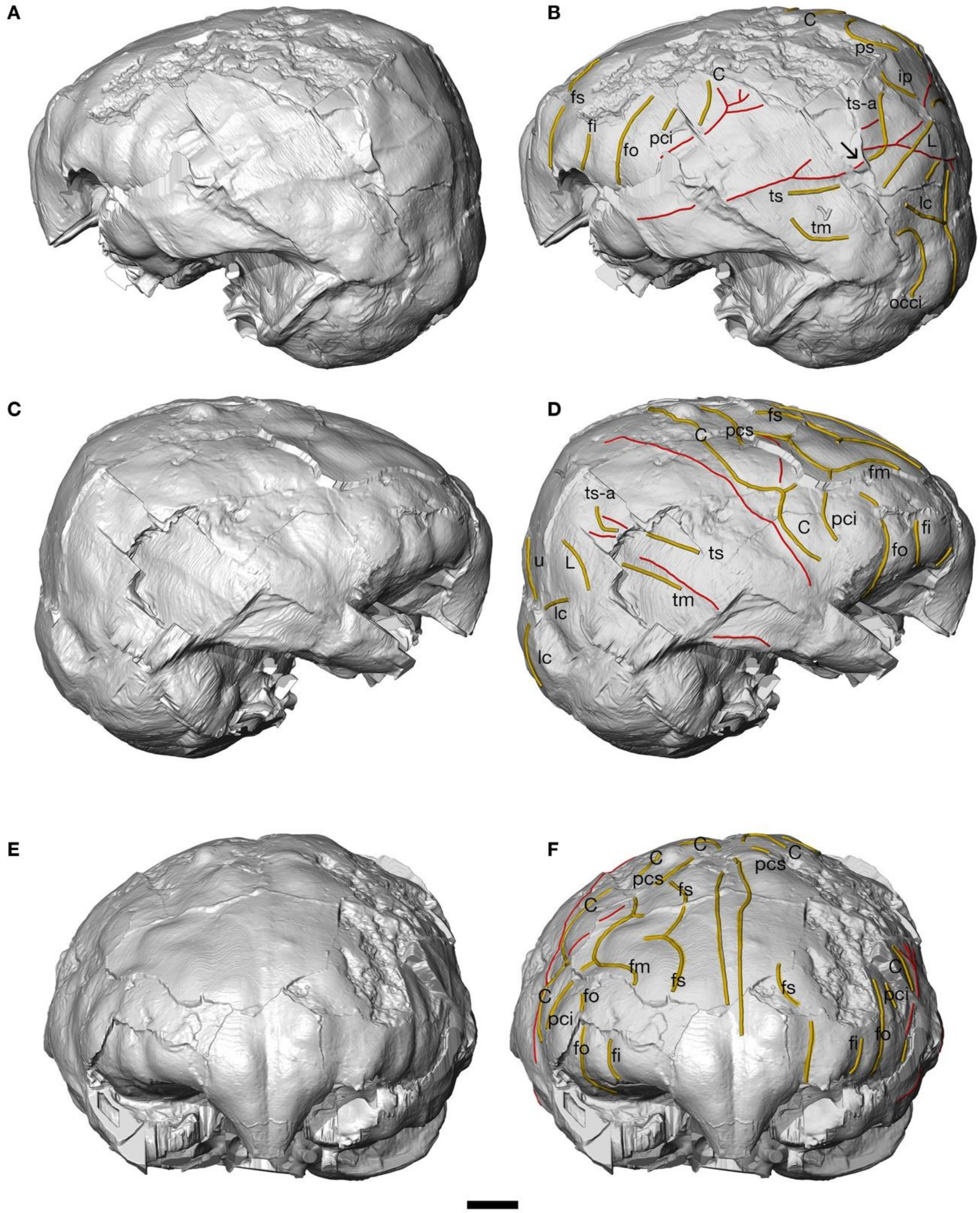

Fig. S3. Natural endocast of DIK-1-1. Lateral views of the unreconstructed DIK-1-1 endocast from the left (**A, B**) and the right (**C**, **D**) side, as well as in frontal view (**E, F**). Sulci are drawn as yellow lines, blood vessels as red lines. The arrow in (B) points to a blood vessel disrupted by the taphonomic displacement of the posterior part of the skull. C *sulcus centralis*, fs *frontalis superior*, fm *frontalis medius*, fi *frontalis inferior*, fo *fronto-orbitalis*, h horizontal ramus of pci, ip *s. intraparietalis*, pci *praecentralis inferior*, pcs *praecentralis superior*, ps *parietalis superior*, pti *postcentralis inferior*, ptm *postcentralis medius*, pts *postcentralis superior*, L *s. lunatus*, ts *temporalis superior*, ts-a *ramus temporalis superior*, tm *temporalis medius*, occi *occipitalis inferior*, lc s. *calcarinus lateralis*, u *s. calcarinus ramus superior.* Scale bar is 1 cm.

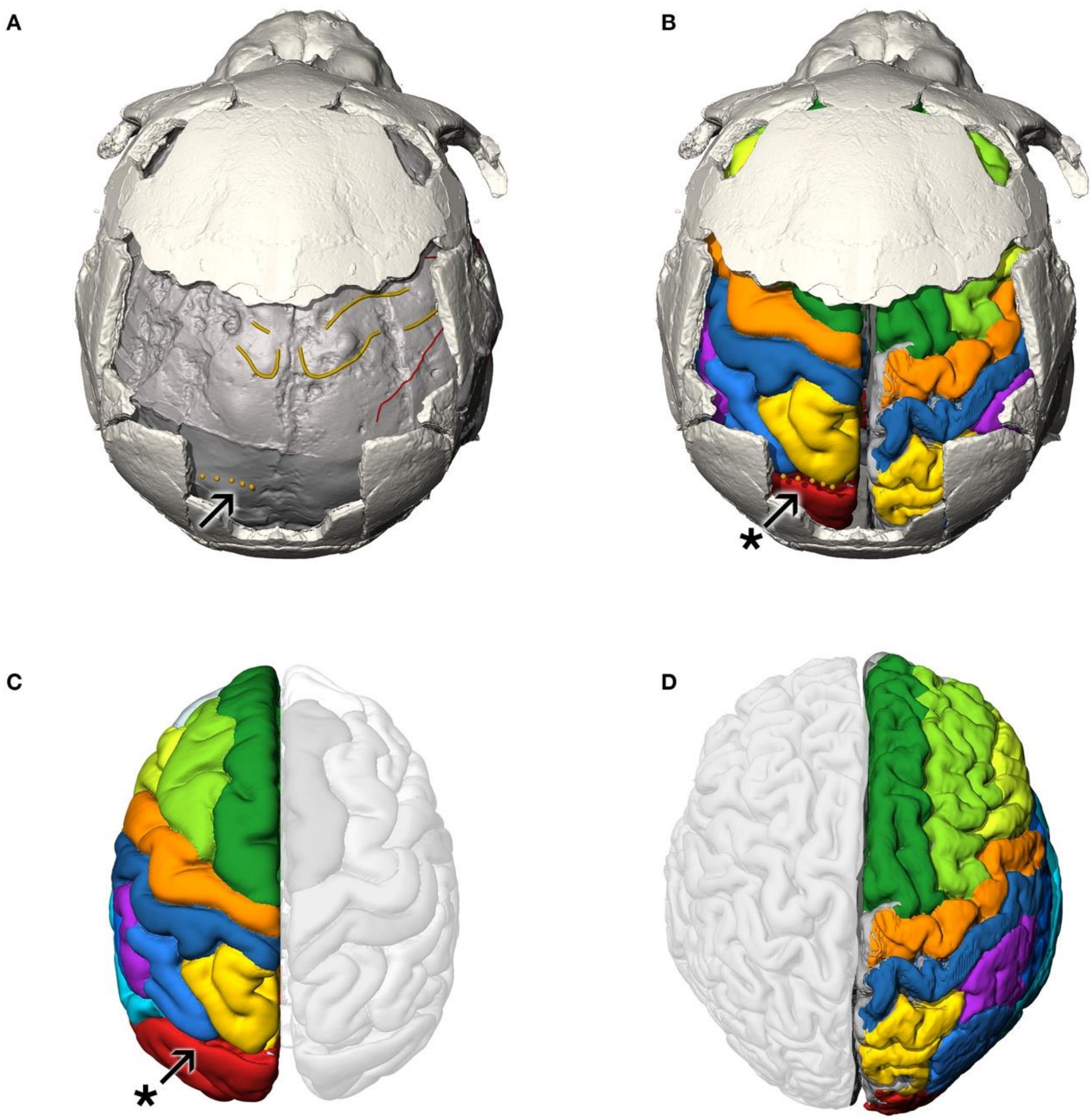

Fig. S4. Ape-like lunate sulcus in DIK-1-1. (**A**) The reconstructed DIK-1-1 endocast shows a clear impression of a lunate sulcus (L; shown as an orange dotted line). (**B**) Thin-plate spline warping the left hemisphere of a chimpanzee brain (**C**) and the right hemisphere of a human brain (**D**) to match the neurocranial shape of the DIK-1-1 reconstruction shows that its lunate sulcus matches the chimpanzee prediction perfectly (arrow with asterisk). Morphology and position of the lunate sulcus in DIK-1-1 are therefore ape-like.

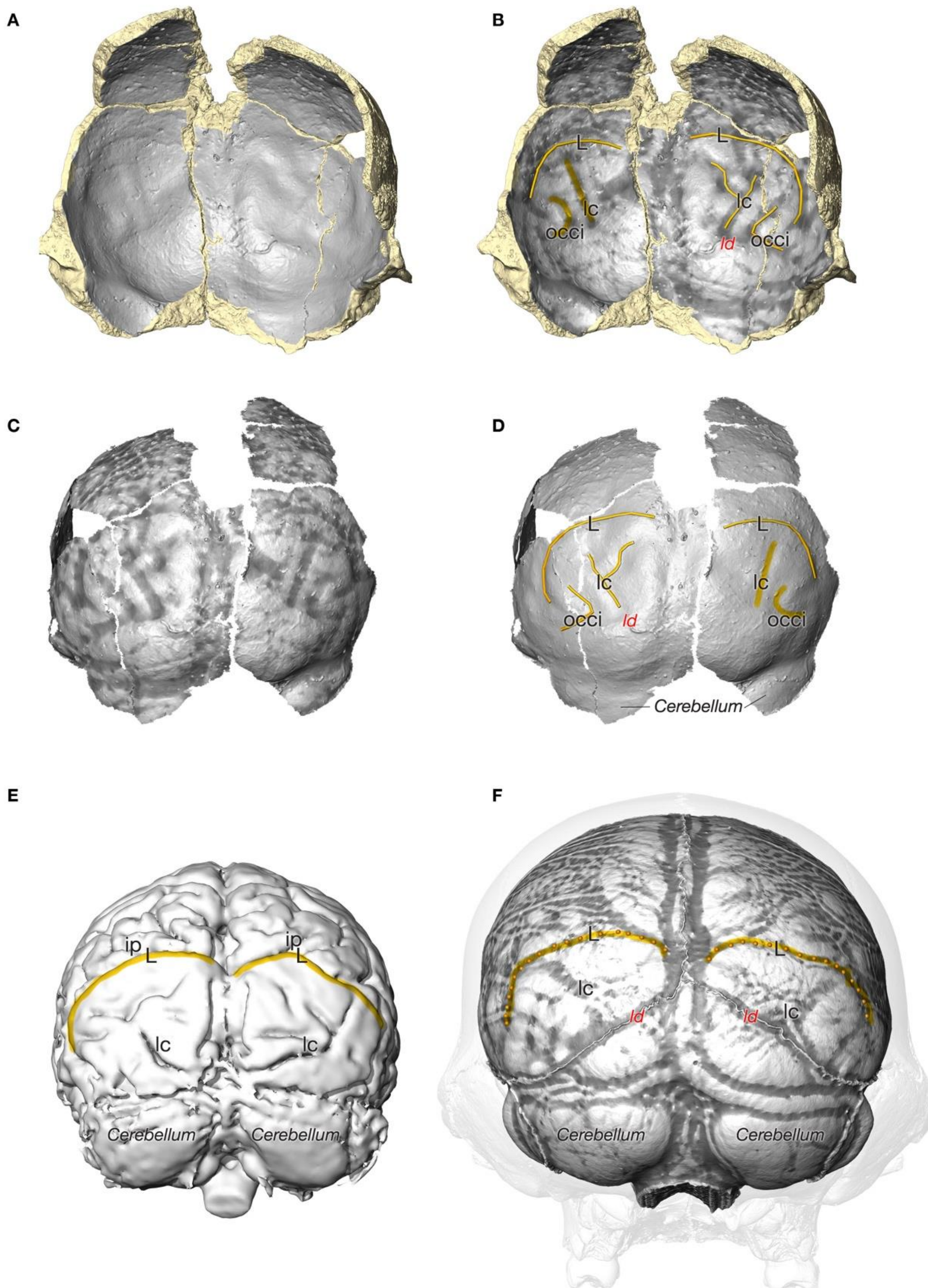

Fig. S5. Endocranial morphology of A.L. 162-28. The micro-CT data of the specimen reveal a clear impression of an ape-like lunate sulcus (L) on the left and right side. Sulcal labels as in Fig. 3; *ld*: lambdoidal suture. (**A, B**) Anterior view. The endocranial surface is shown in gray. (**C, D**) Posterior view of the endocranial surface. (**E**) Posterior view of a chimpanzee brain based on an in-vivo MRI scan ("Amanda" from the Yerkes National Primate Research Center). (**F**) Chimpanzee endocast based on a post-mortem CT scan (*Pan troglodytes verus* from the Taï forest). In (B, C, F) we superimposed a grayscale gradient based on the local curvature to visually enhance the sulcal impressions.

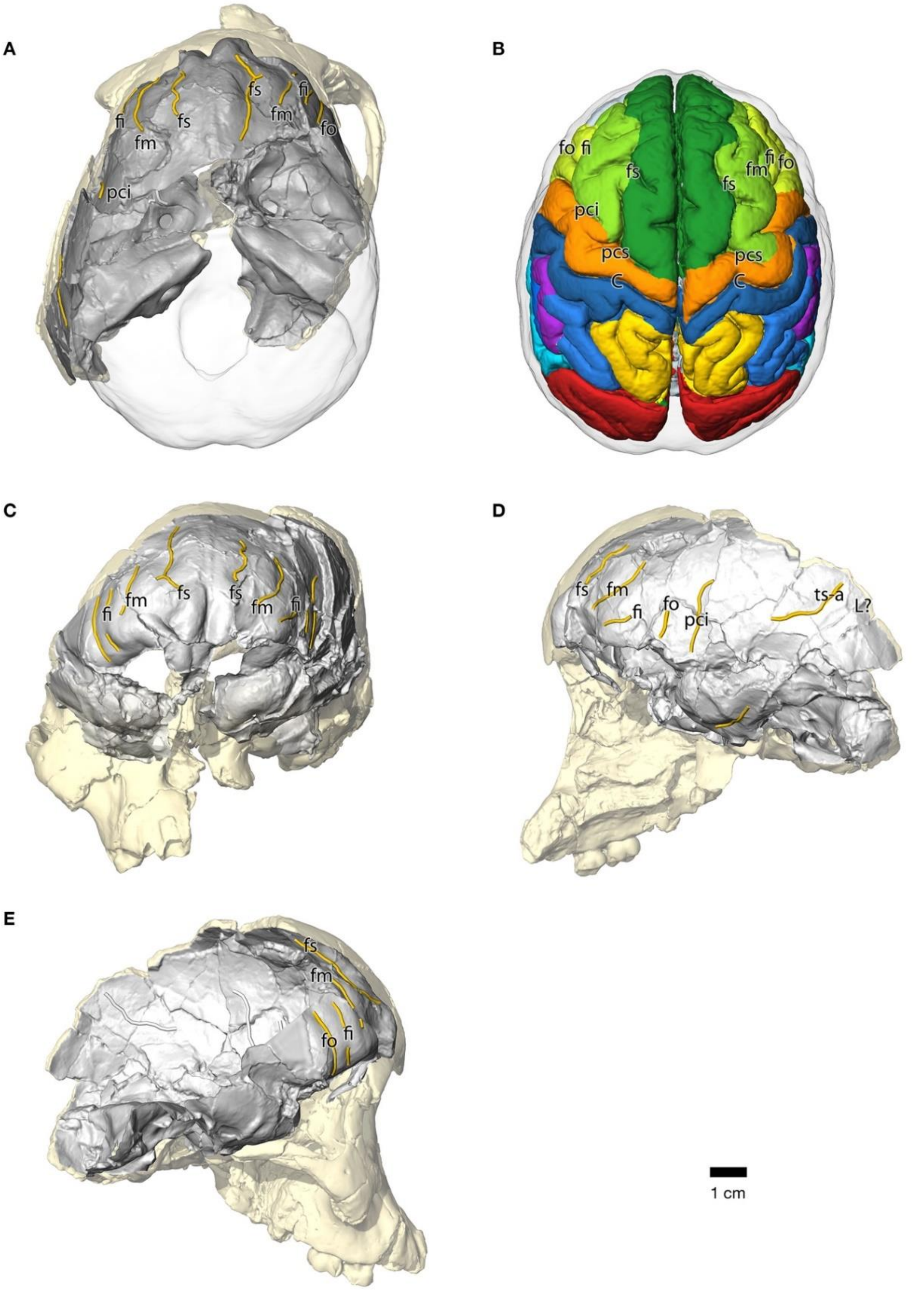

Fig S6. Endocast of A.L. 333-105. (**A**) Superior view of the unreconstructed endocast of A.L. 333-105. Sulci are drawn as yellow lines (for labels see Methods section). Semitransparent gray surface shows outline of reconstructed endocasts. The original bone is also shown as a beige semitransparent surface. (**B**) superior view of an infant *Pan troglodytes* brain from MRI data and an endocasts (semitransparent surface) from CT data of the same individual. Colors approximate the boundaries between major convolutions of the brain. (**C-E**) as in (A) showing frontal, left lateral and right lateral views, respectively. Gray lines in (E) show *ts-a*, *pci*, and part of *fo* on the opposite (left) side. Scale bar is 1 cm.

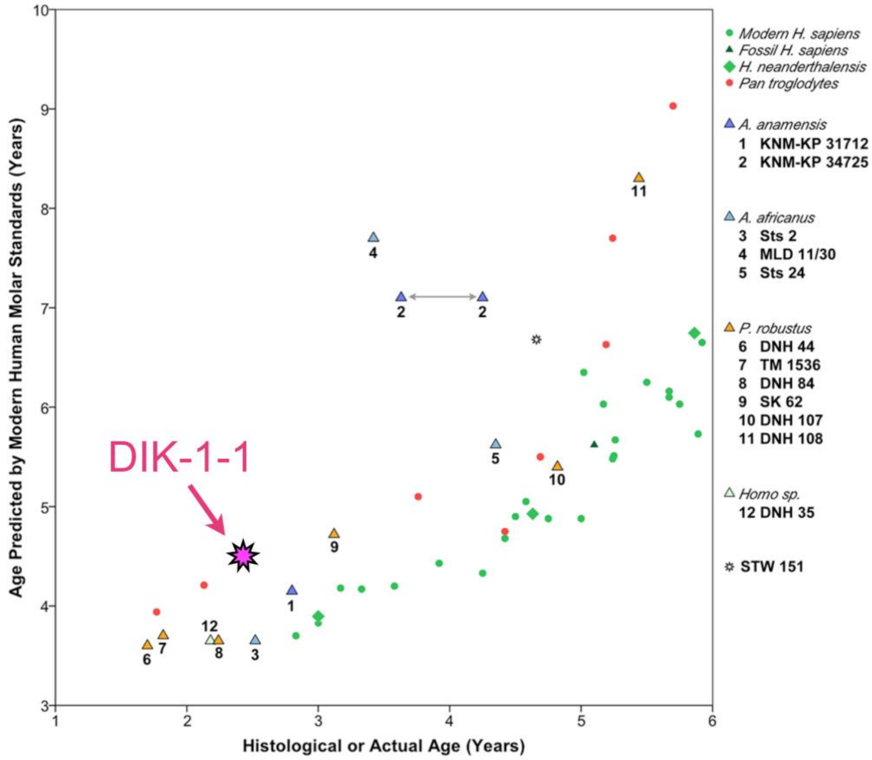

Fig. S7. Ages predicted from modern human molar calcification standards compared to known- or histologically-derived ages. DIK-1-1 is plotted as a pink star. The method and comparative sample are described in (*23*).

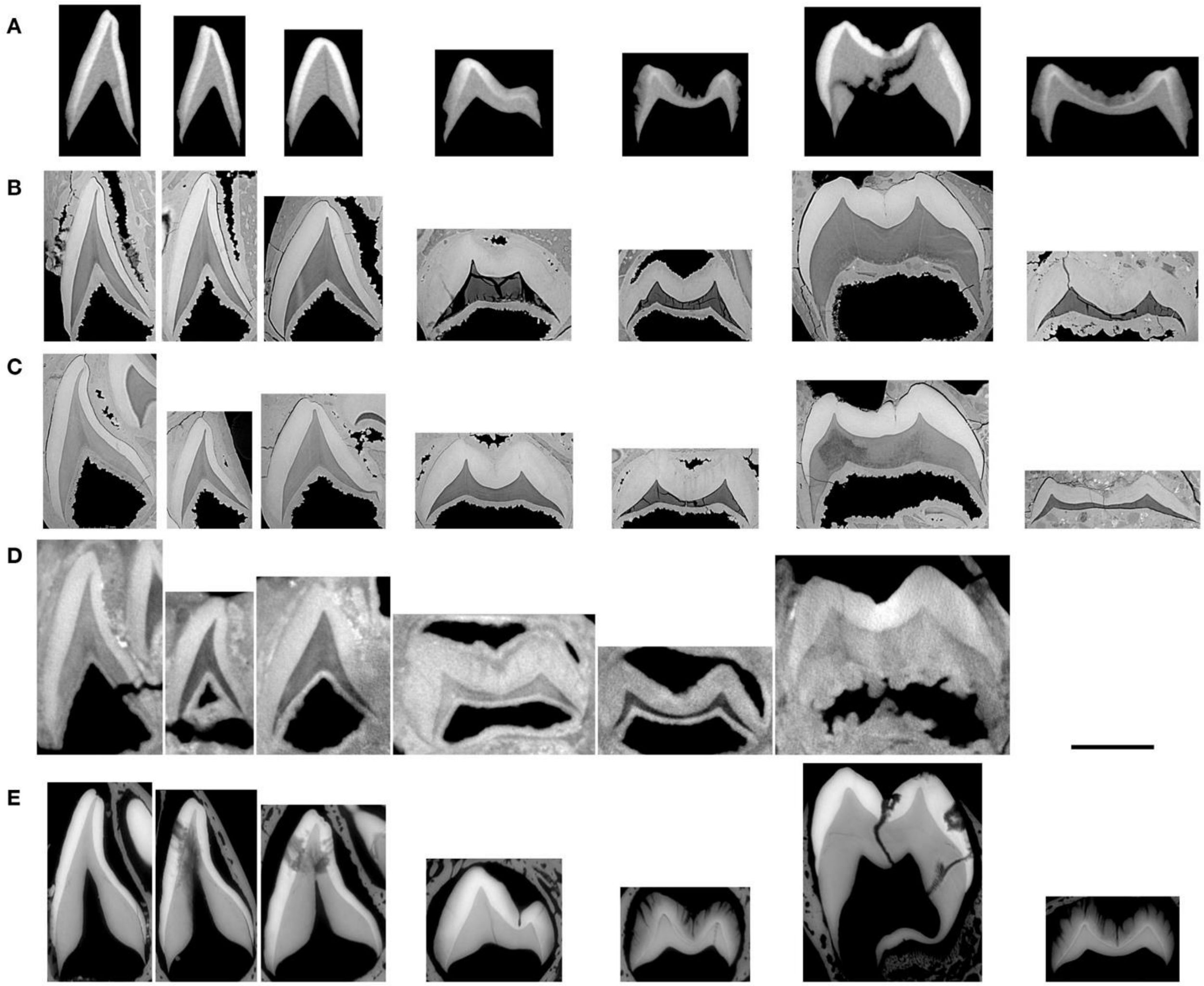

Fig S8. Chimpanzee-equivalent age at death estimation. Teeth from left to right: I1, I2, C, P3, P4, M1, M2. (**A**) Lower permanent teeth of a *P. troglodytes verus* specimen from the Taï Forest, Ivory Coast (MPI-EVA 06/16 [11777], Bambou), aged 2.13 years at death. The specimen was imaged using a Skyscan 1173 microtomograph. (**B**, **C**) Lower and upper permanent teeth of DIK-1-1 (*A. afarensis*), respectively, imaged at the ESRF, on the ID19 beamline. (**D**) Upper permanent teeth of A.L. 333-105 (*A. afarensis*), imaged with a Skyscan 1173 microtomograph. The M2 is not preserved. Both *A. afarensis* specimens are similar to the chimpanzee in overall developmental stage and pattern. However, in enamel thickness and overall dental shape they more closely resemble modern humans, justifying the use of the thick enamel model for score conversion from micro CT slices to radiographs. (**E**) Lower permanent teeth of a modern human (CCEC-30001165, musée des Confluences, Lyon), imaged at the ESRF beamline BM05. Comparison of modern and fossil specimens shows that fossilization has substantially modified the original degree of mineralization of the dental germs: incomplete crowns appear to be fully mineralized (e.g., P4s and M2s), and normal density gradients are not visible at the developing cervix of all other teeth. Scale is 5 mm.

Table S1. Comparative data for lower first molar metaconid crown formation times.

	Time in Days (Max– Min)	Source
A. afarensis (DIK-1-1)	603	This study
A. afarensis (A.L. 333-52)	737	(*60*)
P. troglodytes	633 (601–682)	(*61*)
H. neanderthalensis	846 (788–885)	(*37*)
Early SA *Homo* sp.	876	(*23*)
G. gorilla	888 (714–1004)	(*23*)
H. sapiens (recent)	930 (842-990)	(*37*)

Table S2. Technical parameters. Synchrotron scanning of DIK-1-1 at the ESRF.

Voxel size (µm)	45.7	30.3	4.94	0.678	0.678
Sample	complete skull	complete skull / dental developmental level	permanent teeth dental germ	LLI1 enamel long period lines periodicity	LLI1 enamel long period lines periodicity
Beamline	ID17	ID19	ID19	ID19	ID19
Optic	45 µm taper optic ID17 with cerium doped taper protection	30 µm Hasselblad optic from ID19	5 µm Rodenstock optic ID19	Optic Peter revolver with 10x 0.3 N.A. and 2x eyepiece	Optic Peter revolver with 10x 0.3 N.A. and 2x eyepiece
Date	March 2010	March 2010	March 2010	March 2010	March 2010
Average energy (keV)	70	100	~71	60	60
Filters (mm)	vitreous carbon 2.56 Al 4.2 Cu 2	vitreous carbon 2.56 Al 4.2 Cu 2	Diamond 1mm Al 2mm Cu 1mm	Diamond 1mm Al 2 mm Cu 0.14 mm	Diamond 1mm Al 2 mm Cu 0.14 mm
Propagation distance (mm)	4500	5000	5000	150	150
Monochromator	Si 111 curved double Laue	Si 111 curved double Laue	polychromatic beam	single bounce multilayer W/B4C 2.5 nm	single bounce multilayer W/B4C 2.5 nm
Sensor	FReLoN 2K14 (*62*)	FReLoN 2K14 (*62*)	FReLoN 2K14	FReLoN 2K14	FReLoN 2K14
Camera mode	Frame transfer mode, no shutter	Frame transfer mode, no shutter	Frame transfer mode, no shutter	Full Frame, mechanical X-ray shutter	Full Frame, mechanical X-ray shutter
Scintillator	Gadox 60	LuAG:Ce 750 µm	Gadox 5 µm	GGG:Eu 20 µm	GGG:Eu 20 µm
Insertion device (ID)	W150+W125	W150	W150	U32	U32
ID Gap (mm)	25 / 40	27	65	11.5	11.5
Machine filling mode	16 bunches (max 90 mA)	16 bunches (max 90 mA)	16 bunches (max 90 mA)	16 bunches (max 90 mA)	16 bunches (max 90 mA)
Number of Projections	3999	5000	6000	2499	5000
References every N projections	3499	5000	6000	100	250
Scan geometry	360 degrees, step by step scan, vertical series, absorption protocol with glass balls (*36*)	360 degrees, half acquisition, step by step scan, vertical series, double scan	360 degrees, half-acquisition, continuous scan, vertical series	360 degrees, vertical series, continuous scan	360 degrees, half-acquisition, continuous scan
Exposure time (s)	0.15	0.1	0.3	0.7	1
Time per scan (min)	22.28	23.00	40.43	41.86	100.61
Number of scans	40	62	92	5	2
Reconstruction	modified Paganin delta/beta 1000 + ring correction (*63, 64*)	modified Paganin delta/beta 1000 + ring correction (*63, 64*)	edge detection	Paganin delta/beta 50 (for denoising only)	Paganin delta/beta 50 (for denoising only)

Data file S1. SI_Gunz_et_al_Dental_Scoring. Dental score conversion from microtomographic to radiographic data.

REFERENCES AND NOTES

1. S. R. Leigh, Brain growth, life history, and cognition in primate and human evolution. *Am. J. Primatol.* **62**, 139–164 (2004).

2. Z. Cofran, Brain size growth in Australopithecus. *J. Hum. Evol.* **130**, 72–82 (2019).

3. S. C. McFarlin, S. K. Barks, M. W. Tocheri, J. S. Massey, A. B. Eriksen, K. A. Fawcett, T. S. Stoinski, P. R. Hof, T. G. Bromage, A. Mudakikwa, M. R. Cranfield, C. C. Sherwood, Early brain growth cessation in wild virunga mountain gorillas (*Gorilla beringei beringe*i). *Am. J. Primatol.* **75**, 450–463 (2013).

4. S. L. Robson, B. Wood, Hominin life history: Reconstruction and evolution. *J. Anat.* **212**, 394–425 (2008).

5. J. J. Hublin, S. Neubauer, P. Gunz, Brain ontogeny and life history in Pleistocene hominins. *Philos. Trans. R Soc. Lond. B Biol. Sci.* **370**, 20140062 (2015).

6. H. Coqueugniot, J.-J. Hublin, F. Veillon, F. Houët, T. Jacob, Early brain growth in Homo erectus and implications for cognitive ability. *Nature* **431**, 299–302 (2004).

7. T. Sakai, A. Mikami, M. Tomonaga, M. Matsui, J. Suzuki, Y. Hamada, M. Tanaka, T. Miyabe-Nishiwaki, H. Makishima, M. Nakatsukasa, T. Matsuzawa, Differential prefrontal white matter development in chimpanzees and humans. *Curr. Biol.* **22**, 171 (2012).

8. E. Armstrong, K. Zilles, M. Curtis, A. Schleicher, Cortical folding, the lunate sulcus and the evolution of the human brain. *J. Hum. Evol.* **20**, 341–348 (1991).

9. A. A. de Sousa, C. C. Sherwood, H. Mohlberg, K. Amunts, A. Schleicher, C. E. MacLeod, P. R. Hof, H. Frahm, K. Zilles, Hominoid visual brain structure volumes and the position of the lunate sulcus. *J. Hum. Evol.* **58**, 281–292 (2010).

10. R. L. Holloway, D. Broadfield, M. S. Yuan, *The Human Fossil Record, Brain Endocasts—The Paleoneurological Evidence*, J. H. Schwartz, I. Tattersall, Eds. (John Wiley & Sons, 2004), vol. 3.

11. Z. Alemseged, F. Spoor, W. H. Kimbel, R. Bobe, D. Geraads, D. Reed, J. G. Wynn, A juvenile early hominin skeleton from Dikika, Ethiopia, *Nature* **443**, 296–301 (2006).

12. Z. Cofran, J. M. DeSilva, A neonatal perspective on *Homo erectus* brain growth. *J. Hum. Evol.* **81**, 41–47 (2015).

13. R. L. Holloway, Cerebral brain endocast pattern of *Australopithecus afarensis* hominid. *Nature* **303**, 420–422 (1983).

14. S. R. Leigh, Brain ontogeny and life history in Homo erectus. *J. Hum. Evol.* **50**, 104–108 (2006).

15. D. Falk, Hadar AL 162-28 endocast as evidence that brain enlargement preceded cortical reorganization in hominid evolution. *Nature* **313**, 45–47 (1985).

16. R. L. Holloway, W. H. Kimbel, Endocast morphology of Hadar hominid AL 162-28. *Nature* **321**, 536 (1986).

17. D. Falk, Endocast morphology of Hadar hominid AL 162-28—Reply. *Nature* **321**, 536–537 (1986).

18. D. Falk, C. P. E. Zollikofer, M. Ponce de León, K. Semendeferi, J. L. Alatorre Warren, W. D. Hopkins, Identification of in vivo sulci on the external surface of eight adult chimpanzee brains: Implications for interpreting early hominin endocasts. *Brain Behav. Evol.* **91**, 45–58 (2018).

19. R. L. Holloway, S. D. Hurst, H. M. Garvin, P. T. Schoenemann, W. B. Vanti, L. R. Berger, J. Hawks, Endocast morphology of Homo naledi from the Dinaledi Chamber, South Africa, *Proc. Natl. Acad. Sci. U.S.A.* **115**, 5738–5743 (2018).

20. R. L. Holloway, Revisiting the South African Taung australopithecine endocast: The position of the lunate sulcus as determined by the stereoplotting technique. *Am. J. Phys. Anthropol.* **56**, 43–58 (1981).

21. W. H. Kimbel, Y. Rak, The cranial base of Australopithecus afarensis: New insights from the female skull. *Philos. Trans. R Soc. Lond. B Biol. Sci.* **365**, 3365–3376 (2010).

22. A. Le Cabec, N. Tang, P. Tafforeau, Accessing developmental information of fossil hominin teeth using new synchrotron microtomography-based visualization techniques of dental surfaces and interfaces. *PLOS ONE* **10**, e0123019 (2015).

23. T. M. Smith, P. Tafforeau, A. L. Cabec, A. Bonnin, A. Houssaye, J. Pouech, J. Moggi-Cecchi, F. Manthi, C. Ward, M. Makaremi, C. G. Menter, Dental ontogeny in pliocene and early pleistocene hominins. *PLOS ONE* **10**, e0118118 (2015).

24. J. M. DeSilva, A shift toward birthing relatively large infants early in human evolution. *Proc. Natl. Acad. Sci. U.S.A.* **108**, 1022–1027 (2011).

25. K. Rosenberg, W. Trevathan, Birth, obstetrics and human evolution. *BJOG* **109**, 1199–1206 (2002).

26. J. M. DeSilva, J. J. Lesnik, Brain size at birth throughout human evolution: A new method for estimating neonatal brain size in hominins. *J. Hum. Evol.* **55**, 1064–1074 (2008).

27. R. G. Tague, C. O. Lovejoy, AL 288-1—Lucy or Lucifer: Gender confusion in the Pliocene. *J. Hum. Evol.* **35**, 75–94 (1998).

28. J. M. Desilva, N. M. Laudicina, K. R. Rosenberg, W. R. Trevathan, Neonatal Shoulder Width Suggests a Semirotational, Oblique Birth Mechanism in Australopithecus afarensis. *Anat. Rec.* **300**, 890–899 (2017).

29. H. M. Dunsworth, A. G. Warrener, T. Deacon, P. T. Ellison, H. Pontzer, Metabolic hypothesis for human altriciality. *Proc. Natl. Acad. Sci. U.S.A.* **109**, 15212–15216 (2012).

30. M. E. Pereira, S. R. Leigh, Modes of primate developement, in *Primate Life Histories and Socioecology*, P. M. Kappeler, M. E. Pereira, Eds. (University of Chicago Press, 2003), pp. 149–176.

31. K. Isler, C. P. van Schaik, Allomaternal care, life history and brain size evolution in mammals. *J. Hum. Evol.* **63**, 52–63 (2012).

32. W. H. Kimbel, Y. Rak, D. C. Johanson, *The Skull of* Australopithecus afarensis (Human Evolution Series, Oxford Univ. Press, 2004).

33. W. H. Kimbel, D. C. Johanson, Y. Coppens, Pliocene hominid cranial remains from the Hadar Formation, Ethiopia. *Am. J. Phys. Anthropol.* **57**, 453–499 (1982).

34. W. H. Kimbel, L. K. Delezene, "Lucy" redux: A review of research on australopithecus afarensis. *Am. J. Phys. Anthropol.* **140**, 2–48 (2009).

35. P. Gunz, P. Mitteroecker, S. Neubauer, G. W. Weber, F. L. Bookstein, Principles for the virtual reconstruction of hominin crania. *J. Hum. Evol.* **57**, 48–62 (2009).

36. K. J. Carlson, D. Stout, T. Jashashvili, D. J. de Ruiter, P. Tafforeau, K. Carlson, L. R. Berger, The endocast of MH1, *Australopithecus sediba*. *Science* **333**, 1402–1407 (2011).

37. T. M. Smith, P. Tafforeau, D. J. Reid, J. Pouech, V. Lazzari, J. P. Zermeno, D. Guatelli-Steinberg, A. J. Olejniczak, A. Hoffman, J. Radovčić, M. Makaremi, M. Toussaint, C. Stringer, J.-J. Hublin, Dental evidence for ontogenetic differences between modern humans and Neanderthals. *Proc. Natl. Acad. Sci. U.S.A.* **107**, 20923–20928 (2010).

38. K. L. Kuykendall, Dental development in chimpanzees (*Pan troglodytes*): The timing of tooth calcification stages. *Am. J. Phys. Anthropol.* **99**, 135–157 (1996).

39. R. S. Lacruz, M. C. Dean, F. Ramirez-Rozzi, T. G. Bromage, Megadontia, striae periodicity and patterns of enamel secretion in Plio-Pleistocene fossil hominins. *J. Anat.* **213**, 148–158 (2008).

40. F. Spoor, P. Gunz, S. Neubauer, S. Stelzer, N. Scott, A. Kwekason, M. C. Dean, Reconstructed *Homo habilis* type OH 7 suggests deep-rooted species diversity in early *Homo*. *Nature* **519**, 83–86 (2015).

41. S. Neubauer, P. Gunz, G. W. Weber, J. J. Hublin, Endocranial volume of *Australopithecus africanus*: New CT-based estimates and the effects of missing data and small sample size. *J. Hum. Evol.* **62**, 498–510 (2012).

42. S. Neubauer, J. J. Hublin, P. Gunz, The evolution of modern human brain shape. *Sci. Adv.* **4**, eaao5961 (2018).

43. P. Gunz, P. Mitteroecker, F. L. Bookstein, Semilandmarks in three dimensions, in *Modern Morphometrics in Physical Anthropology, Developments in Primatol: Progress and Prospect*, D. E. Slice, Ed. (Kluwer Academic/Plenum Publishers, 2005), pp. 73–98.

44. P. Gunz, P. Mitteroecker, Semilandmarks: A method for quantifying curves and surfaces. *Hystrix* **24**, 103–109 (2013).

45. N. Scott, S. Neubauer, J. J. Hublin, P. Gunz, A shared pattern of postnatal endocranial development in extant hominoids. *Evol. Biol.* **41**, 572–594 (2014).

46. S. Neubauer, P. Gunz, U. Schwarz, J.-J. Hublin, C. Boesch, Brief communication: Endocranial volumes in an ontogenetic sample of chimpanzees from the Taï Forest National Park, Ivory Coast. *Am. J. Phys. Anthropol.* **147**, 319–325 (2012).

47. S. Neubauer, P. Gunz, J.-J. Hublin, The pattern of endocranial ontogenetic shape changes in humans. *J. Anat.* **215**, 240–255 (2009).

48. J. G. Herndon, J. Tigges, D. C. Anderson, S. A. Klumpp, H. M. Mcclure, Brain weight throughout the life span of the chimpanzee. *J. Comp. Neurol.* **409**, 567–572 (1999).

49. J. DeSilva, J. Lesnik, Chimpanzee neonatal brain size: Implications for brain growth in *Homo erectus*. *J. Hum. Evol.* **51**, 207–212 (2006).

50. A. H. Schultz, The relative size of the cranial capacity in primates. *Am. J. Phys. Anthropol.* **28**, 273–287 (1941).

51. K. Isler, E. Christopher Kirk, J. M. A. Miller, G. A. Albrecht, B. R. Gelvin, R. D. Martin, Endocranial volumes of primate species: Scaling analyses using a comprehensive and reliable data set. *J. Hum. Evol.* **55**, 967–978 (2008).

52. F. Marchand, *Über das Hirngewicht des Menschen* (B.G. Teubner, 1902).

53. S. M. Blinkov, I. I. Glezer, *The Human Brain in Figures and Tables: A Quantitative Handbook* (Plenum Press and Basic Books, 1968).

54. C. Dean, B. Wood, in *Digital Archives of Human Paleobiology*, L. Bondioli, R. Macchiarelli, Eds. (Consiglio Nazionale delle Ricerche, ADS Solutions, 2003).

55. C. A. Lockwood, W. H. Kimbel, D. C. Johanson, Temporal trends and metric variation in the mandibles and dentition of *Australopithecus afarensis*. *J. Hum. Evol.* **39**, 23–55 (2000).

56. C. J. Conolly, *External Morphology of the Primate Brain* (Charles C. Thomas, 1950).

57. A. Klein, J. Tourville, 101 labeled brain images and a consistent human cortical labeling protocol. *Front. Neurosci.* **6**, 171 (2012).

58. A. Gómez-Robles, W. D. Hopkins, C. C. Sherwood, Modular structure facilitates mosaic evolution of the brain in chimpanzees and humans. *Nat. Commun.* **5**, 4469 (2014).

59. A. Gómez-Robles, W. D. Hopkins, S. J. Schapiro, C. C. Sherwood, Relaxed genetic control of cortical organization in human brains compared with chimpanzees. *Proc. Natl. Acad. Sci. U.S.A.* **112**, 14799–14804 (2015).

60. R. S. Lacruz, F. V. Ramirez Rozzi, Molar crown development in *Australopithecus afarensis*. *J. Hum. Evol.* **58**, 201–206 (2010).

61. T. M. Smith, P. Tafforeau, D. J. Reid, R. Grün, S. Eggins, M. Boutakiout, J.-J. Hublin, Earliest evidence of modern human life history in North African early *Homo sapiens*. *Proc. Natl. Acad. Sci. U.S.A.* **104**, 6128–6133 (2007).

62. J.-C. Labiche, O. Mathon, S. Pascarelli, M. A. Newton, G. G. Ferre, C. Curfs, G. Vaughan, A. Homs, D. F. Carreiras, Invited article: The fast readout low noise camera as a versatile x-ray detector for time resolved dispersive extended x-ray absorption fine structure and diffraction studies of dynamic problems in materials science, chemistry, and catalysis. *Rev. Sci. Instrum.* **78**, 091301 (2007).

63. D. Paganin, S. C. Mayo, T. E. Gureyev, P. R. Miller, S. W. Wilkins, Simultaneous phase and amplitude extraction from a single defocused image of a homogeneous object. *J. Microsc.* **206**, 33–40 (2002).

64. S. Sanchez, P. E. Ahlberg, K. M. Trinajstic, A. Mirone, P. Tafforeau, Three-dimensional synchrotron virtual paleohistology: A new insight into the world of fossil bone microstructures. *Microsc. Microanal.* **18**, 1095–1105 (2012).